SUPPORTING INFORMATION

for

Recurrent mismatch binding by MutS mobile clamps on DNA localizes repair complexes nearby

Pengyu Hao[1], Sharonda J. LeBlanc[1,2], Brandon C. Case[3], Timothy C. Elston[4,5], Manju M. Hingorani[3], Dorothy A. Erie[2,6*], Keith R. Weninger[1*]

[1] Department of Physics, North Carolina State University, Raleigh, NC 27695

[2] Department of Chemistry, University of North Carolina, Chapel Hill, NC 27599

[3] Molecular Biology and Biochemistry Department, Wesleyan University, Middletown, CT 06459

[4] Department of Pharmacology, University of North Carolina, Chapel Hill, NC 27599

[5] Computational Medicine Program, University of North Carolina at Chapel Hill, Chapel Hill, NC 27599

[6] Lineberger Comprehensive Cancer Center, University of North Carolina at Chapel Hill, Chapel Hill, NC 27599

Includes:

Supporting table S1

Supporting figures S1-S6

Supporting methods

www.pnas.org/cgi/doi/10.1073/pnas.1918517117

	DNAs with 1 MutS	Total DNAs	% DNA occupied at start of observation	Related Figure
No treatment	199	960	20.7 %	S1A
ATP -> nothing	187	2030	9.2 %	-
ATP -> ATP	182	1849	9.8 %	1G, 2A, 3A, S1B
ATP -> ADP	236	2337	10.1 %	2B
ATP -> ATPγS	75	771	9.7 %	2C
ATP -> ADP+ATPγS	202	2272	8.9 %	2D

Table S1. Characterization of occupancy of DNA by MutS at the beginning of observations for various experimental conditions. The observations began 2-4 minutes following the final buffer exchange. Columns report (left to right), buffers used in washes, number of DNA colocalized with one MutS, total DNA interrogated, calculated percent of DNA occupied by one MutS, and reference to related figures. In the row indicated "No treatment", MutS is added with no nucleotide and no exchange to subsequent buffer containing nucleotides is executed, and thus represents the occupancy of MutS on DNA before adding ATP to form mobile clamps. In the other rows, occupancies are reported for experiments that used the protocol in Figure 1E where MutS was added in buffer with no added nucleotide, followed by a first buffer wash with ATP to create mobile clamps and a subsequent buffer exchange to a final buffer containing the specified nucleotides. Given that 2-4 minutes elapsed between the final buffer exchange and commencement of observation, the consistent occupancy under the various buffers suggests that the mobile clamps have lifetimes on the DNA under these various conditions longer than a few minutes. Accordingly, the disappearance of donor fluorescence in our individual molecule intensity time traces (Figure 1F) is likely due to donor photobleaching rather than MutS dissociation.

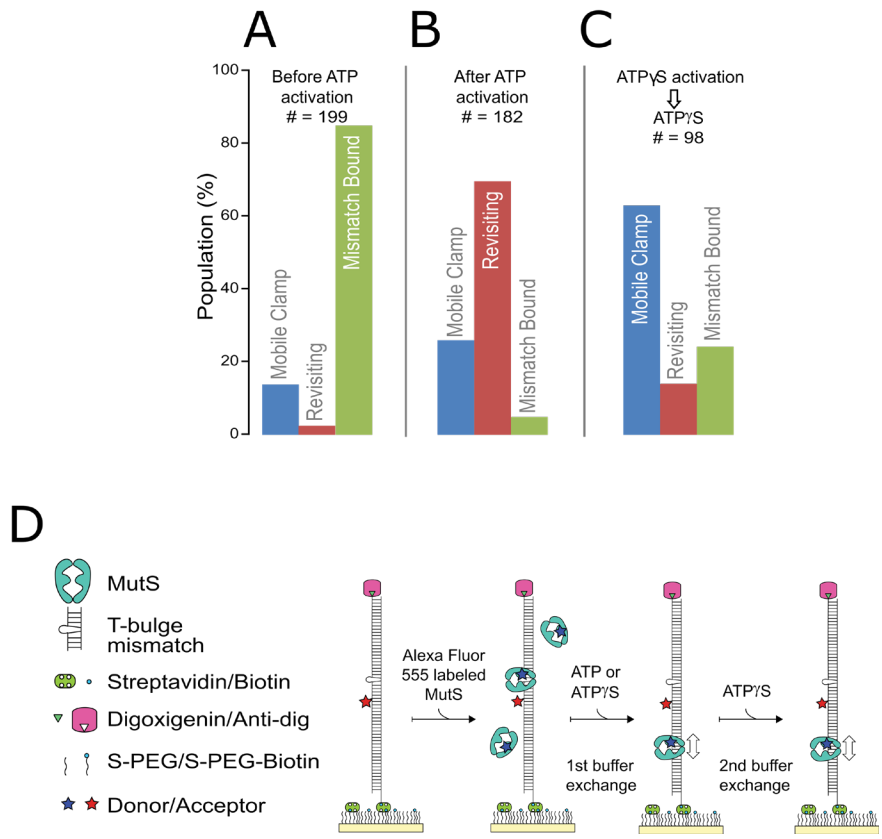

Figure S1. Development of the assay for detection of MutS on DNA optimized for a maximum of one mobile clamp per end-blocked DNA. Color bars are as defined in Figure 1F. (A) MutS was added to the T-bulge DNA channel in buffer without nucleotide. In this condition, over 80% of MutS exhibits stable, non-switching FRET (green bar), as expected for a long-lived mismatch bound state that does not convert to a mobile clamp. The presence of one MutS at the mismatch suppresses additional MutS from loading on the DNA. (B) Upon the first exchange to buffer containing ATP, excess MutS is removed from the channel solution (schematic in panel D). After the addition of ATP, 95% of the MutS that remains bound is in a mobile clamp state, with some bypassing (FRET 0, blue bar) and most revisiting the mismatch one or more times (FRET switching between 0 and 0.5, red bar). Only 5% remains bound at the mismatch exhibiting a stable signal (FRET 0.7, green bar). (C) Similar experiment to panel B, but with ATP-γ-S in the first buffer exchange to create MutS mobile clamps, followed by a second buffer exchange with ATP-γ-S. Now, 70% of mismatch-bound MutS converts to mobile clamps, but most of these clamps have zero FRET (mismatch bypassing population, blue bar), confirming that ATP-γ-S supports MutS transition from mismatch-bound to mobile clamp state, but it does not support rebinding of the mobile clamp to the mismatch (small revisiting population, red bar). (D) Schematic of experiments with end-blocked DNA: addition of MutS without nucleotide, first buffer exchange (no additional MutS) introducing ATP (panel B) or ATP-γ-S (panel C) (no additional MutS), and second buffer exchange introducing ATP-γ-S (panel C).

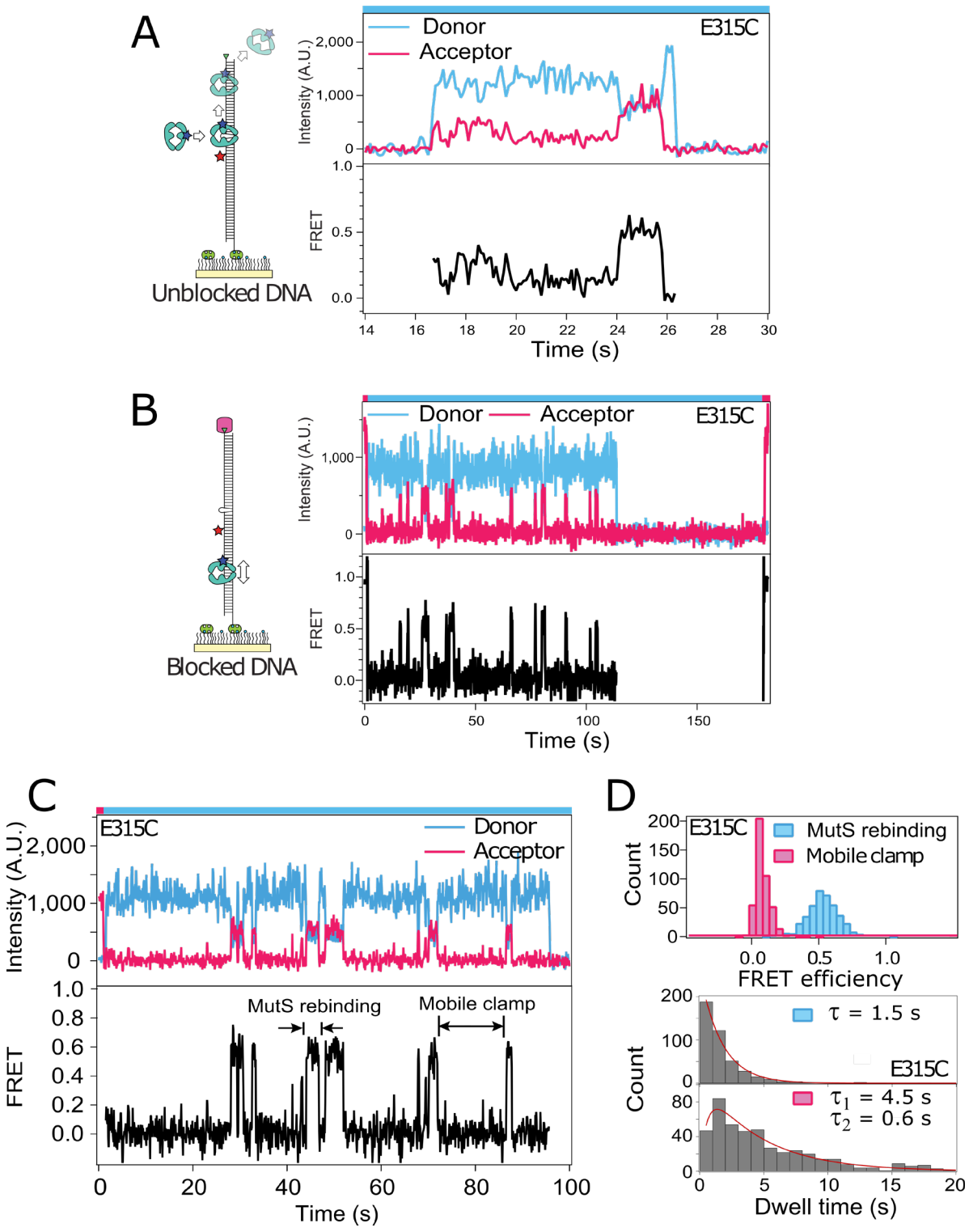

Figure S2. MutS mobile clamp labeled with AF555 at E315C shows rebinding to a T-bulge mismatch in 2 mM ATP buffer with comparable kinetics to MutS labeled at M88C (see Figure 1 for results with AF555-MutS (M88C)). **(A)** Example time trace of donor and acceptor emission

(top) and FRET (bottom) for AF555-MutS (E315C) on unblocked DNA. In contrast to MutS-M88C (Figure 1), binding of MutS-E315C to the mismatch results in FRET 0.2, consistent with the relative locations of the donor and acceptor dyes; however, the intermediate state for both proteins shows similar FRET 0.5. **(B)** Time trace showing rebinding events of AF555-MutS (E315C) on end-blocked DNA. **(C)** Zoomed in view of a trace showing the mobile clamp revisiting the mismatch. **(D)** FRET histogram (top) and dwell time distributions for AF555-MutS (E315C) rebinding events on blocked DNA. Red lines are fits to the dwell time distributions (methods). We previously determined the lifetime of the intermediate FRET 0.5 state on pathway to mobile clamp formation to be 1.2 s (1). Notably, when the MutS-E315C mobile clamp rebinds the mismatch, it adopts a state with similar FRET efficiency and lifetime as the intermediate state when it first forms a clamp and leaves the mismatch (see panel A), as seen also with MutS-M88C. Color bars on top of the intensity vs. time graphs indicate laser illumination color (red = 640 nm; blue = 532 nm).

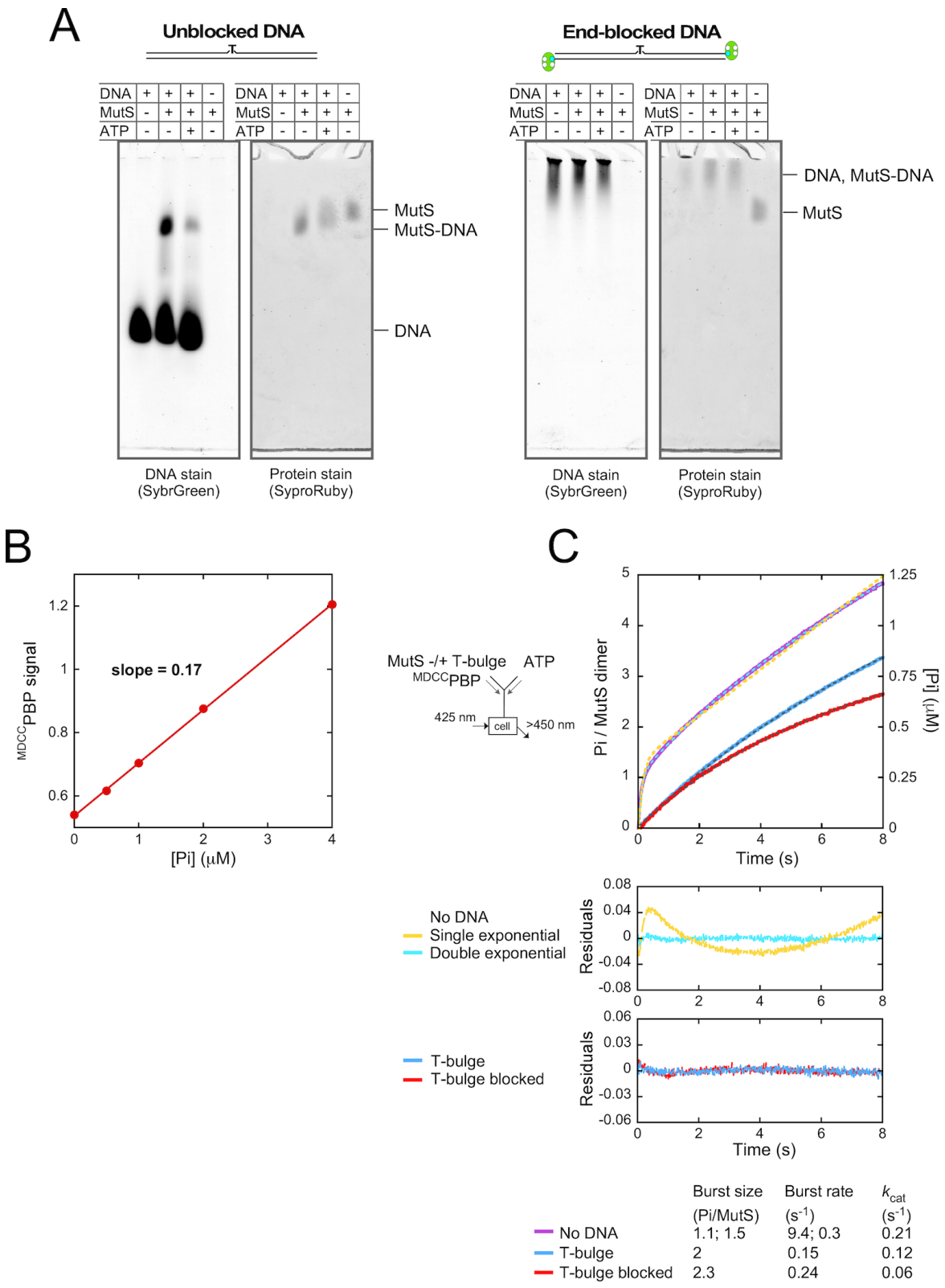

Figure S3. MutS binding and ATPase activity as a mobile clamp on T-bulge DNA. **(A)** A non-denaturing gel mobility shift assay shows MutS binding to unblocked and doubly end-blocked T-bulge DNA. Upon addition of ATP, MutS slips off unblocked DNA but is retained on end-

blocked DNA. **(B)** A calibration plot of ^{MDCC}PBP fluorescence versus Pi concentration used to determine the amount of Pi produced in the pre-steady state ATPase experiments. **(C)** Pi release data from Figure 2E are shown here again to illustrate that MutS ATPase kinetics in the absence of DNA (purple trace) are best fit is to a double exponential + linear (cyan dashed line) rather than a single exponential + linear equation (yellow dashed line; residuals plotted below). The burst amplitudes and rates from the fit reveal asymmetric activity of the two ATPase sites on MutS, with one hydrolyzing ATP ~30-fold faster (9.4 s^{-1}) than the other (0.3 s^{-1}), followed by slow steady state turnover (the amplitudes and rate constants are listed below the graph). In contrast, MutS ATPase kinetics with end-blocked DNA (red trace) are best fit by a single exponential + linear equation (residuals plotted below), which reveals that both sites on the MutS mobile clamp hydrolyze ATP at a slow rate of 0.24 s^{-1} and undergo steady state turnover, while it is trapped on DNA.

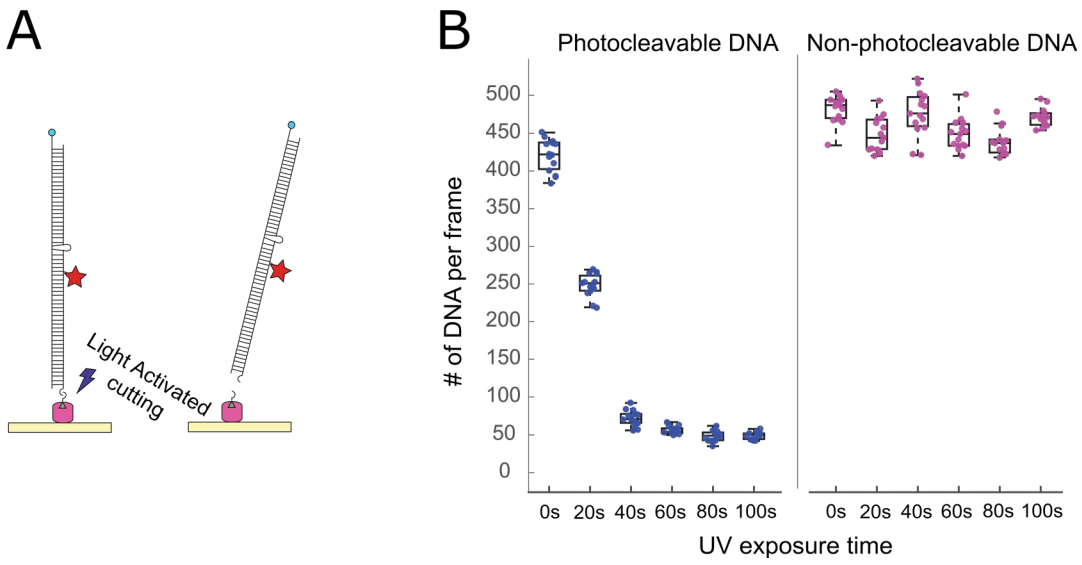

Figure S4. Characterization of photocleavage for unblocking of DNA substrates. **(A)** Schematic of experiments with Cy5-T-bulge DNA substrates modified by digoxigenin on one end and biotin on the other, surface-tethered by anti-digoxigenin adsorbed on a bare quartz slide. **(B)** The sample was illuminated with a red laser to detect Cy5 fluorescence. The number of DNAs per 60 μm x 120 μm area of view on the TIRF microscope was counted before and after UV exposure for increasing durations. UV-induced cleavage to release the digoxigenin group breaks the link between the DNA and the surface, allowing DNA to diffuse away and become undetectable by total internal reflection fluorescence (TIRF) microscopy. DNA loss (left graph) occurs within 20 seconds of UV exposure and saturates at about 80% loss in less than 90 seconds of exposure. When the surface tether is not cleavable (no photocleavable link between DNA and digoxigenin), there is no appreciable loss of DNA even after 100 sec UV exposure (right graph). The individual dots represent the numbers of DNA measured from each field of view. Many fields of view were sampled on one slide for each condition and box plots characterize those populations (the median is the central line in box, the 75th and 25th percentiles are the upper and lower edges of the box, and the most extreme values are marked by the bars). Independent replicates using additional slides yielded similar results (not shown). Note, this result also demonstrates that the 90 sec, 365 nm UV exposure does not harm the Cy5 fluorophore.

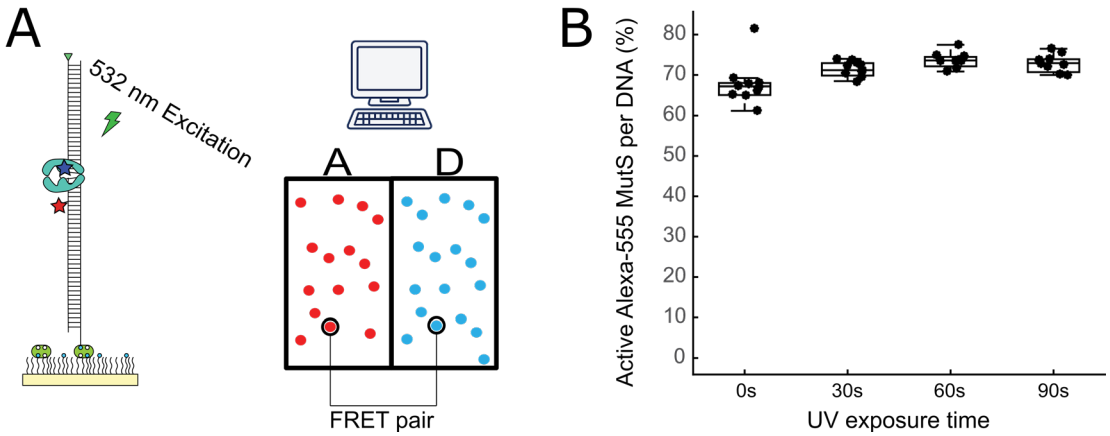

Figure S5. UV exposure does not bleach the AF555 fluorophore on MutS. **(A)** Schematic of experiment showing AF555-MutS (M88C) bound to the Cy5-T-bulge DNA (without the photocleavable link) in buffer without nucleotide. The DNA was located by Cy5 emission under red laser excitation. AF555-MutS at the mismatch was identified by FRET efficiency >0.5 under green illumination. **(B)** The fraction of DNA with mismatch-bound MutS does not decrease under UV exposure (used for photocleavage in Figure S4) even at 90 seconds. Each individual dot represents the percent of identified acceptor-labeled DNA on the surface that colocalize with a donor-MutS in a state leading to FRET greater than 0.5 for one field of view in a channel. The populations across many fields of view on one slide are characterized by the collection of dots and by the box plots as in Figure S4.

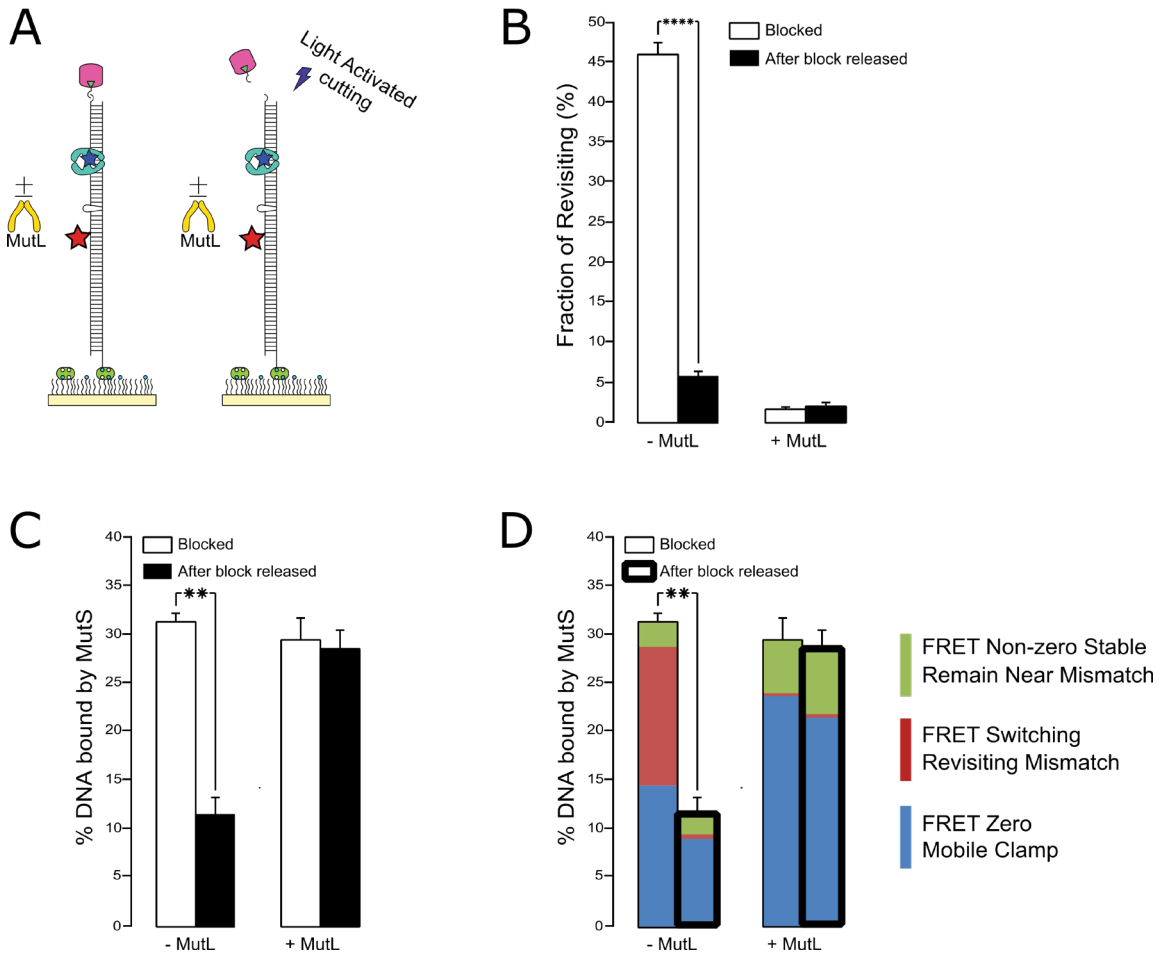

Figure S6. Additional characterization of the effect of MutL on MutS mobile clamps (see Figure 3A-D). **(A)** Schematic of experiment using photocleavage to release the end-block on DNA. **(B)** The bars report the fraction of revisiting MutS (switching between FRET 0 and 0.5, as in middle trace in Figure 1F, red bars in Figure 1G, 2A-D, 3A-B) observed on DNA with the end-block and after its removal, in the absence and presence of MutL. Loss of the MutS revisiting fraction with MutL even on end-blocked DNA indicates that MutS mobile clamp motion is arrested by MutL. Error bars are s.e.m. from 3 experiments; **** indicates $p \leq 0.0001$ for 2-sample unpaired t-test; two-tailed p value (p=0.0001). **(C)** Reproduction of Figure 3D for direct comparison with the following panel. **(D)** The same results as Figure 3D and panel C, but with the subpopulations of the 3 types of events defined and color coded with the same key as in Fig 1F: Blue=FRET zero (bypassing clamp); Red=FRET switching between 0 and 0.5 (revisiting clamp); Green=FRET non-zero, stable (mismatch-bound MutS). In both C and D, error bars are s.e.m. from 3 experiments; ** indicates $p \leq 0.005$ for 2-sample unpaired t-test; two-tailed p value (p=0.005).

Supporting methods

DNA substrates:

The construction of mismatched DNA substrates has been described in detail elsewhere (2). Briefly, a 5'-biotin modified primer and a 5'-digoxigenin modified primer were used for PCR from a plasmid to generate a 550 basepair, linear, double stranded DNA with modified ends. A segment of single stranded DNA was removed from the middle of the 550 basepair double strand DNA using a nicking enzyme, heating to 70 °C, and then purifying with PCR cleanup kit while still warm. A single stranded oligo insert that matches the gapped region with the exception of an inserted T (T-bulge) mismatch and Cy5 fluorophore, was then annealed to cover the gap. The nicks were then sealed by repeated ligation reactions as described previously, where efficiency was determined to be >80% (2). Given that 70% of the DNA molecules show revisiting in the presence of ATP (Figure 2A), it is highly unlikely that nicks induce hydrolysis and revisiting capability in MutS. To make photocleavable DNA, we purchased a modified oligonucleotide from Integrated DNA Technologies with an internal photocleavable group (called Int PC Spacer; /iSpPC/) between the last 5'base and the digoxigenin group in the digoxigenin modified primer (5'-/5DigN/iSpPC/ GAG TCA GTG AGC GAG GAA GC-3').

For the ensemble ATPase experiments, 3′-biotin modified DNA strands were purchased desalted and HPLC purified from Integrated DNA Technologies (template: 5′-CCA GCT GAG GCC TGG CTG AGG ATT GCT GAG GAA TTC ACC G/3BiodT/-3′; T-bulge complement: 5′-CGG TGA ATT CCT CAG CAA TCT CTC AGC CAG GCC TCA GCT GG/3BiodT/-3′). To prepare duplex DNA, the two strands were annealed in 1:1 ratio by heating for 1 min at 95 °C and cooling O/N to room temperature in buffer (20 mM Tris–HCl, pH 7.8, 100 mM sodium acetate); >95% duplex was confirmed by non-denaturing PAGE. To prepare double end-blocked DNA, the duplex was incubated with neutravidin in 1:2 molar ratio for 15 minutes at room temperature in the same buffer; >95% blocked DNA was confirmed by non-denaturing PAGE (Figure S3A). All nucleotides were purchased from Millipore Sigma.

Proteins:

The expression and purification of *Thermus aquaticus* (*Taq*) MutS and MutL proteins has been described previously (2–5). Two mutant versions of MutS were used in this study for labeling purposes: *Taq* MutS C42A/M88C and *Taq* MutS C42A/E315C. Briefly, wild type and MutS mutants without any tags were expressed in BL21(DE3) *E. coli* cells and were purified by heating the clarified cell lysate to 65 °C for 30 minutes, centrifugation and ammonium sulfate precipitation of the supernatant, centrifugation and resuspension of the pellet, followed by Q-Sepharose chromatography. MutS (M88C or E315C) was labeled with Alexa Fluor 555-maleimide (AF555) with labeling efficiency ranging from 60% to 100%. Free dye was removed by gel-filtration through Sephadex G50. We have previously verified the mismatch binding affinity and ATPase activity of these MutS mutants is similar to wild type *Taq* MutS (1, 2).

Taq MutL without any tag was expressed in BL21(DE3) *E. coli* cells and purified by ammonium sulfate precipitation of clarified cell lysate, followed by heparin (HiTrap) chromatography of the resuspended pellet, as described previously (2).

Peg surface passivation:

Quartz slides (with drilled holes) and glass cover slips were cleaned by sonicating sequentially in acetone, ethanol and 1M potassium hydroxide and stored in ultrapure water. Methoxy-Poly (Ethylene Glycol)–Silane (mPEG-Silane, MW 2000) and Biotin-Poly (Ethylene Glycol)-Silane (Biotin-PEG-Silane, MW 3400) (Laysan Bio, Inc.) were used to passivate the slide surface to prevent non-specific binding. PEG-silane stocks were aliquoted into 20 mg (non-biotin) and 2 mg (biotin) quantities in a nitrogen-purged glove box. For treating a microscope slide, 2 mg of biotin-PEG-silane was dissolved in 10 μL 0.1 M sodium bicarbonate solution and 20 mg mPEG was dissolved in 80 μL 0.1 M sodium bicarbonate solution. 1μL of the biotin-PEG solution was then added into the 80 μL mPEG solution. The mixture was briefly vortexed and centrifuged to remove air bubbles. The solution was then applied to the quartz slide and the glass cover slip was placed on top of the slide, sandwiching the solution in the area to be used in the chamber. After overnight incubation in a humid box to prevent the solution from drying out, the slide/cover slip sandwich was opened and the surfaces were extensively rinsed with ultrapure water. Both quartz slide and glass cover slip were dried in air. A second application of mPEG-silane using the same method (omitting the biotin-PEG-silane) was then performed, which further reduced non-specific binding. For experiments, flow chambers were assembled between the passivated quartz slide and coverslip using double sided tape and 5 minute epoxy, as described previously (1, 2, 6).

smFRET assay using end-blocked DNA:

The prism-type total internal reflection, single molecule fluorescence microscope and our data analysis routines have been described previously (1, 2, 6, 7). All single molecule fluorescence experiments were performed at 22 °C. Candidate molecules are identified based on red fluorescence from Cy5-labeled immobilized DNA under 1 second of red laser illumination. Next, green laser illumination is applied for an extended time to excite AF555-labeled MutS, while donor and acceptor intensities are measured from locations containing single DNA molecules with a 60x/1.2N.A./water immersion objective (Olympus), a Dualview image splitter (Photometrics) and an emCCD (Cascade512B, Photometrics) recording 10 frames per second. Each movie ends with a few seconds of observation with red laser illumination to assess the final state of the acceptor. Color bars on the top of the intensity vs. time graphs indicate laser illumination color (red = 640 nm illumination; blue = 532 nm illumination). FRET efficiency was calculated as $E = I_A/(I_A+I_D)$ where I_A and I_D are background and leakage corrected acceptor and donor intensities, respectively. Dwelltimes of states for kinetic analyses and FRET histograms of states were measured by hand. Lifetimes were deduced from dwelltime histograms by fitting to single exponential decay functions (Fig 1D, Fig. 1I-FRET 0.5 population, and SI

Appendix Fig. S2D-FRET 0.5 population) or to a two-step kinetic model given by $k_1k_2(\exp(-k_2t) - \exp(-k_1t))/(k_1 - k_2)$ where k_1 and k_2 are the two kinetic rates (Fig. 1I-FRET 0 population, and SI Appendix Fig. S2D-FRET 0 population). As discussed elsewhere, lifetimes less than around 2 sec derived from the two-step model applied to data acquired with our experimental parameters can have large errors (1).

Characterizing photocleavage-induced release of end-block from DNA

To measure the efficiency of the photocleavage reaction (Figure S4), digoxigenin end-modified Cy5-T-bulge DNA was immobilized on anti-dig molecules adsorbed to a bare quartz surface. DNAs containing photocleavable or non-photocleavable digoxigenin (internal photocleavable spacer omitted) were compared; cleavage releases photocleavable DNA from the surface, resulting in disappearance of the fluorescent spot under 640 nm laser excitation. Specifically, 2 μg/ml anti-dig was applied for 5 minutes to a chamber with an unpassivated quartz surface. Next, the 550 basepair biotin/dig Cy5-T-bulge DNA (either photocleavable or non-photocleavable dig) was applied at low concentration (~10 pM) for 5 minutes to achieve well-spaced immobilized molecules. The chamber was exposed to the UV source (365 nm) for varying times. At each time point, the number of DNA molecules per 60 μm x 120 μm field of view was counted at 15 different locations in the chamber. The results indicate that >88% of DNA molecules with photocleavable digoxigenin are lost after 90 seconds of UV exposure, and there is a negligible effect on DNA with non-photocleavable digoxigenin (Figure S4). Moreover, 90 sec UV light exposure does not photobleach the Cy5 acceptor (Figure S4B, right panel). The possible impact of UV exposure on the AF555 donor was tested using AF555-MutS bound to Cy5-T-bulge DNA (buffer containing no added nucleotide) in a PEG passivated chamber. The DNA was identified by Cy5 emission under red laser excitation, and AF555-MutS at the mismatch was identified by FRET efficiency >0.5 under green illumination. The near constant fraction of DNA with a MutS bound at the mismatch for up to 90 seconds UV exposure indicates AF555 does not photobleach under these conditions (Figure S5).

ATP hydrolysis and Pi release assay with end-blocked DNA

Phosphate (Pi) release from MutS after ATP hydrolysis was measured under pre-steady state conditions by monitoring the increase in fluorescence (λ_{EX} = 425 nm, λ_{EM} > 450 nm) of 7-diethylamino-3-((((2-maleimidyl)ethyl)amino)carbonyl) coumarin-labeled phosphate binding protein (^{MDCC}PBP) on binding free Pi rapidly and with high affinity (10^8 M^{-1} s^{-1}; K_D = 0.1 μM (4, 8)). MutS alone or pre-incubated with unblocked or doubly end-blocked T-bulge DNA was mixed with ATP on a stopped flow instrument in buffer (20 mM Tris–HCl, pH 7.8, 100 mM sodium acetate, 5 mM $MgCl_2$) containing a Pi contaminant mopping system of 0.1 unit/mL polynucleotide phosphorylase (Millipore Sigma) and 0.2 mM 7-methylguanosine (R.I. Chemical Inc., Orange, CA) at 40 °C (final concentrations: 0.25 μM MutS dimer, +/- 0.5 μM end-blocked or unblocked T-bulge DNA, 2 mM ATP and 10 μM ^{MDCC}PBP; T-bulge K_D ~ 20 nM; ATP K_D ~ 1 and 30 μM for the two ATPase sites on MutS) (4). The signal from 4 to 6 traces was averaged

for each experiment, converted to Pi concentration using a calibration curve generated with standard Pi solution (Millipore Sigma) under the same conditions (Figure S3), and corrected for a low background signal at zero time. The data were fit to a double exponential + linear equation ($A_1(1-e^{-k_1 t})+A_2(1-e^{-k_2 t})+k_3 t$); kinetic traces with two burst phases and a linear steady state phase) or a single exponential + linear equation ($A_1(1-e^{-k_1 t})+k_2 t$); kinetic traces with one burst phase and a linear steady state phase) to determine the pre-steady state ATP hydrolysis rate (k_1, k_2) and stoichiometry (A_1, A_2) and the steady state rate (k_{cat} = linear slope/2 sites x [MutS dimer]). The fits are shown as dashed lines in Figure 2E and 2F and Figure S3. The burst stoichiometry (Pi/MutS dimer) and rate constants in Figures 2 and S3 are mean values from 2-3 independent experiments (standard errors of the mean are noted in the Figure 2 legend).

Gel Mobility Shift Assay of MutS-DNA complexes:

Binding of MutS to the unblocked and doubly end-blocked T-bulge DNAs used in ATPase assays was tested using a gel mobility shift assay (Figure S3). 100 nM MutS was incubated with 150 nM unblocked or 200 nM end-blocked DNA in 20 µl buffer (20 mM Tris–HCl, pH 7.8, 100 mM sodium acetate, 5 mM $MgCl_2$) for 10 minutes at 25 °C (reactions containing ATP were incubated for <1 minute). After addition of 3 µl loading dye (glycerol, bromophenol blue), the reactions were run on a 4% polyacrylamide (29:1), 5% glycerol, 5 mM $MgCl_2$ gel in TAE buffer (40 mM Tris acetate, pH 8.3, 1 mM EDTA) at 4 °C and 35 V for ~2 hours. The gel was stained for 30 minutes with 1:1000 dilution of SybrGreen (Thermo Fisher) for DNA, imaged on a Typhoon FLA9000 imager (λ_{EX} = 473 nm, λ_{EM} > 575 nm), and then stained O/N with SyproRuby (Thermo Fisher) for protein and imaged again (λ_{EX} = 473 nm, λ_{EM} > 665 nm).

Construction of the energy landscape (Figure 4A)

We used the average of the rate constants determined for each step in the ordered pathway between initial mismatch recognition and mobile clamp formation (published in Figure 6 of LeBlanc et al. (1)) to calculate the activation free energies of each step using Eyring theory (9): $\Delta G^{\ddagger} = -RTln(\frac{kh}{k_B T})$ where R is the gas constant, T is the temperature, k is the experimental rate constant, h is Planck's constant, k_B is Boltzmann's constant. In LeBlanc *et al.*, 3 states on the pathway to the mobile clamp (State 4) are described: State1: mismatch recognition and accompanying DNA bending (FRET 0.7); State 2: conformational change associated with increased DNA bending but no change in protein-DNA FRET (FRET 0.7*): State 3: additional conformational change associated with decreased DNA bending and lower protein-DNA FRET (FRET 0.5). To estimate the energy differences between states 1 and 2 and between 2 and 3 that occur between initial recognition and first mobile clamp formation (Figure 4A, first three states from the left) we used the ratio of the forward and backward reaction rates. The backward rates have not been well determined, therefore we estimated them based on our observation that approximately 10% of molecules in these states went backwards on the path (1, 3). Specifically, the heights of the transition barriers between states are calculated using average rates from

LeBlanc et al. (1) $k_{1\to2} = 0.31\ s^{-1}$, $k_{2\to3} = 0.55\ s^{-1}$, $k_{3\to4} = 0.74\ s^{-1}$, and the rebinding rate (Figure 1I) $k_{5\to3} = 0.25\ s^{-1}$. The difference between the intermediate state (FRET 0.5, State 3 in Figure 4A) and the mobile clamp state (State 4) in the absence of ATP hydrolysis was calculated assuming the back rate was 0.0017 s^{-1}, based on the 600 s lifetime of the mobile clamp on blocked DNA (10). The observation that MutS mobile clamps can revisit the mismatch in the presence of ATP but not ATP-γ-S indicates that ATP hydrolysis converts MutS mobile clamps (State 4) into a new mobile state (State 5) that can recognize the mismatch. The difference in energy between the rebinding-capable mobile clamp (State 5) and the intermediate (FRET 0.5) state (State 3) was calculated based on the observed rebinding kinetics (Figure 1I).

Estimating the number of times diffusive MutS sliding clamps cross the mismatch between rebinding events

We used diffusion theory to estimate number of times a MutS sliding clamp is expected to cross the mismatch within a time T_{total} between rebinding events (4 seconds, Figure 1I). Consider the DNA to be length $2L$ with the mismatch located at the midpoint. If MutS extends length l along the DNA and moves diffusively with diffusion constant D so that $x(t)$ is the position of the mid-point of MutS at time t, then it encounters the reflecting boundaries of the end-blocked DNA when $x(t) = L - \frac{l}{2}$ or $x(t) = \frac{l}{2} - L$. Note that MutS is on the right side of domain if $x(t) \geq \frac{l}{2}$ and the left side of the domain if $-\frac{l}{2} \geq x(t)$. Suppose that MutS is on the left side of the domain at time t (i.e., $-\frac{l}{2} \geq x(t)$), then a crossing occurs when $x(t + t') \geq \frac{l}{2}$ for the first time. A similar condition holds for crossing from right to left. Also note that immediately after a crossing from left to right occurs, the position of MutS is $x = \frac{l}{2}$.

Let $T(\frac{l}{2})$ be the average time for a crossing to occur, given MutS starts at $\frac{l}{2}$. In this case, the average number of crossings in T_{total} will be given by $\frac{T_{total}}{T(\frac{l}{2})}$. To compute $T(\frac{l}{2})$, we solve the following equation, the first moment (11, 12):

$$D\frac{\partial^2 T(x_o)}{\partial x_o^2} = -1$$

with boundary conditions:

$$T\left(-\frac{l}{2}\right) = 0 \quad \text{and} \quad \frac{\partial T\left(L-\frac{l}{2}\right)}{\partial x_o} = 0$$

The solution is:

$$T(x_o) = \frac{L^2}{2D}\left(1 - \left(\frac{L - \frac{l}{2} - x_o}{L}\right)^2\right)$$

For a starting position of $x_o = \frac{l}{2}$, the solution becomes

$$T\left(\frac{l}{2}\right) = \frac{L^2}{2D}\left(1 - \left(\frac{L-l}{L}\right)^2\right)$$

so the average number of crossings $N_{crossings}$ is given by:

$$N_{crossings} = \frac{T_{total}}{T\left(\frac{l}{2}\right)} = \frac{T_{total}}{\frac{L^2}{2D}\left(1 - \left(\frac{L-l}{L}\right)^2\right)}$$

In our experiments, the DNA is 550 base pairs long $(2L)$ so we use $L = 0.0765$ μm. Two diffusion constants have been reported for *Taq* MutS mobile clamps (3, 13), 0.005 μm^2/s and 0.058 μm^2/s. A lower limit of the extent of MutS on the DNA with in this model (l) is 1 base pair and a conservative maximal estimate is the 8 base pair footprint of *Taq* MutS bound to a T-bulge from the crystal structure (14). Using these ranges for D and l, the number of times that MutS is expected to cross the mismatch during the 4 s between rebinding events is between 98 and 8940.

Supporting information references

1. S. J. LeBlanc, *et al.*, Coordinated protein and DNA conformational changes govern mismatch repair initiation by MutS. *Nucleic Acids Res.* **46**, 10782–10795 (2018).
2. R. Qiu, *et al.*, MutL traps MutS at a DNA mismatch. *Proc. Natl. Acad. Sci.* **112**, 10914–10919 (2015).
3. R. Qiu, *et al.*, Large conformational changes in MutS during DNA scanning, mismatch recognition and repair signalling. *EMBO J.*, 1–13 (2012).
4. E. Antony, M. M. Hingorani, Asymmetric ATP binding and hydrolysis activity of the Thermus aquaticus MutS dimer is key to modulation of its interactions with mismatched DNA. *Biochemistry* **43**, 13115–13128 (2004).
5. A. Sharma, C. Doucette, F. N. Biro, M. M. Hingorani, Slow conformational changes in MutS and DNA direct ordered transitions between mismatch search, recognition and signaling of DNA repair. *J. Mol. Biol.* **425**, 4192–205 (2013).
6. J. W. Gauer, *et al.*, "Single-Molecule FRET to Measure Conformational Dynamics of DNA Mismatch Repair Proteins" in *Methods in Enzymology*, (2016), pp. 285–315.
7. L. E. Sass, C. Lanyi, K. Weninger, D. A. Erie, Single-molecule FRET TACKLE reveals highly dynamic mismatched DNA-MutS complexes. *Biochemistry* **49**, 3174–3190 (2010).
8. M. Brune, *et al.*, Mechanism of Inorganic Phosphate Interaction with Phosphate Binding Protein from Escherichia coli. *Biochemistry* **37**, 10370–10380 (1998).
9. K. J. Laidler, M. C. King, Development of transition-state theory. *J. Phys. Chem.* **87**, 2657–2664 (1983).

10. C. Jeong, *et al.*, MutS switches between two fundamentally distinct clamps during mismatch repair. *Nat. Struct. Mol. Biol.* **18**, 379–385 (2011).
11. S. Redner, *A Guide to First-Passage Processes* (Cambridge University Press, 2001).
12. C. W. Gardiner, *Handbook of Stochastic Methods for Physics, Chemistry and the Natural Sciences* (Springer-Verlag, 1990).
13. W.-K. Cho, *et al.*, ATP Alters the Diffusion Mechanics of MutS on Mismatched DNA. *Struct. Des.*, 1–11 (2012).
14. G. Obmolova, C. Ban, P. Hsieh, W. Yang, Crystal structures of mismatch repair protein MutS and its complex with a substrate DNA. *Nature* **407**, 703–710 (2000).